Organic Electronics 83 (2020) 105738

Contents lists available at ScienceDirect

Organic Electronics

journal homepage: http://www.elsevier.com/locate/orgel

High absorption coefficient π-conjugation-extended donor-acceptor copolymers for ternary-blend solar cells

Hyeongjin Hwang [1], Chaneui Park [1], Dong Hun Sin [1], Eunjoo Song, Kilwon Cho [**]

Department of Chemical Engineering, Pohang University of Science and Technology, Pohang, 37673, South Korea

ARTICLE INFO

Keywords:
High absorption coefficient copolymers
Donor-acceptor copolymers
π-Conjugation extension
Ternary-blend solar cells

ABSTRACT

The effects of one-dimensional (1D) and two-dimensional (2D) π-conjugation extensions of donor–acceptor (D–A) copolymers on their intrinsic and photovoltaic properties in ternary-blend organic solar cells (OSCs) were investigated systematically by using one polymer donor and two acceptors ($PC_{71}BM$, ITIC). A series of wide bandgap D–A copolymers (PBT-OTTs) were synthesized based on the benzo[1,2-b:4,5-b′]dithiophene (BDT) unit and the thieno[3,4-c]pyrrole-4,6(5H)-dione (TPD) unit, which extend in the backbone (1D) and side-group directions (2D) respectively from the PBT-OTT backbone. These copolymers are **PBT-OTT** (the parent polymer), **PDTBT-OTT** (with a 1D backbone extension consisting of dithieno[2,3-d; 2′,3′-d′]benzo[1,2-b; 4,5-b′]dithiophene), **PTTBT-OTT** (with a 2D side group extension consisting of 2-alkyl thieno[3,2-b]thiophene (TT)), and **PBTBT-OTT** (with a 2D side group extension consisting of 2-alkyl benzo[b]thiophene (BT)). Light absorption is significantly increased in the case of **PBTBT-OTT** due to its extended 2D π-conjugation length and high crystallinity. This increase results from the extended delocalization length and the increased absorption coefficient α of **PBTBT-OTT**. The wide bandgap polymer **PBTBT-OTT** has the highest α of the series, so the complementary absorption of the low bandgap ITIC means that the ternary-blend OSCs based on **PBTBT-OTT** exhibit the highest $J_{SC} = 16.61$ mA cm^{-2} and PCE = 8.61%. We believe that these findings provide systematic guidelines for the π-conjugation extension of conjugated polymers and thus the design of high-efficiency ternary-blend OSCs.

1. Introduction

Organic solar cells (OSCs) are inexpensive, lightweight, flexible, and amenable to solution-based processing for mass production [1–5]. To achieve high power conversion efficiencies (PCEs), much research effort has focused on the design and synthesis of high-efficiency donor and acceptor (D–A) copolymers. The PCEs of single-junction OSCs now exceed 15% [6,7].

Conventional OSCs employ a binary blend of a D–A copolymer as a donor with a fullerene derivative as an acceptor. However, such systems have only a limited capacity to harvest sunlight. To address these limitations, ternary OSCs have been prepared in which a single photoactive layer composed of three absorbing materials, i.e., either wide bandgap (WBG) donors and a low bandgap (LBG) acceptor, or one WBG donor and two LBG acceptors [8–13]. Furthermore, the use of an LBG acceptor and a WBG donor as absorbing materials in the ternary active layer can enable complementary absorption that increases the light-harvesting efficiency and PCE of the OSC [14,15]. High-efficiency ternary-blend OSCs require the blending of appropriate LBG and WBG absorbing materials with $PC_{71}BM$ in a single active layer; the LBG should have an optical bandgap $E_g < 1.8$ eV, and the WBG should have $E_g \geq 1.8$ eV [16].

Recently,3,9-bis(2-methylene-(3-(1,1-dicyanomethylene)-indanone))-5,5,11,11-tetrakis(4-hexylphenyl)-dithieno[2,3-d:2′,3′-d′]-s-indaceno[1,2-b:5,6-b′]dithiophene) (ITIC) has been used as the LBG acceptor because its main absorption band arises near 700 nm ($700 \leq \lambda \leq 800$ nm) and its absorption spectrum complements the spectra of WBG polymers [17]. Moreover, the energy levels of the highest occupied molecular orbital (HOMO) and the lowest unoccupied molecular orbital (LUMO) of ITIC are positioned almost midway between the HOMO and LUMO energy levels of WBG polymers and $PC_{71}BM$; the resulting cascade of energy levels increases the effectiveness of hole and electron charge transfer [18]. However, when ITIC is added to polymer blends, the films typically have poor morphologies due to aggregation [14]. This problem can be solved by adding an appropriate amount of $PC_{71}BM$ to the blend of ITIC with the polymer; the resulting morphologies have optimum phase separation [19]. To effectively

* Corresponding author.
E-mail address: kwcho@postectech.ac.kr (K. Cho).
[1] Joint contributors.

https://doi.org/10.1016/j.orgel.2020.105738
Received 27 December 2019; Received in revised form 4 March 2020; Accepted 24 March 2020
Available online 2 April 2020
1566-1199/© 2020 Elsevier B.V. All rights reserved.

combine the advantages of $PC_{71}BM$ and ITIC, the ratio of ITIC to $PC_{71}BM$ in the ternary-blend layer must be optimized.

To increase the PCEs of ternary-blend OSCs based on an LBG acceptor, a WBG polymer that has a high absorption coefficient α is required. Extending the π-conjugation length of the polymeric backbone can increase its π-electron delocalization, and is therefore an effective way to obtain high α values and to increase the light absorption of OSCs [20]. Therefore, to increase α of the donor polymer, its delocalization length should be extended in one (1D) or two dimensions (2D). For instance, incorporating a thieno[3, 2-b]thiophene (TT) π-bridge as a spacer into the WBG benzodithiophene (BDT)-thienopyrroledione (TPD) backbone significantly increases the 1D π-conjugation length. Hence, in the resulting polymer α is higher and the UV–vis absorption spectrum is red-shifted with respect to that of the parent polymer [21]. Similarly, the fused-ring ladder-type donor moiety indacenodithiophene (IDT) can be extended by fusing two thiophenes to it; this process yields a highly extended seven ring indacenodithienothiophene (IDTT) donor moiety with a 1D π-conjugation extension system [22]. After copolymerizing IDTT with 2F-substituted benzothiadiazole (DFBT), the resulting 1D backbone-extended WBG polymer, PIDTT-DTBT, has a higher α value than the parent polymer, PIDT-DFBT. Finally, to extend the 2D π-conjugation length of the WBG polymeric backbone, oligothienyl π-conjugated structures can be introduced as side groups into the donor moiety BDT and the resulting BDT derivatives then copolymerized with DFBT units [23]. This 2D π-conjugation extension significantly increases the intensity of the UV–vis light absorption band of the corresponding polymer.

Herein, with the aim of synthesizing a WBG polymer with high α, we selected **PBT-OTT** [19] as the parent polymer, which is a copolymer of the BDT derivative as the donor moiety and the TPD derivative as the acceptor moiety, and systematically extended its polymer chains by adding aromatic compounds in a 1D linear arrangement (**PDTBT-OTT**) or a 2D planar arrangement (**PTTBT-OTT** and **PBTBT-OTT**) (Scheme 1 and Table S1). **PBT-OTT** is a good photovoltaic material when it is paired as the donor polymer with ITIC and $PC_{71}BM$ in ternary-blend OSCs; under optimized device conditions, PCE = 8.18%; the optimized overall acceptor ratio of ITIC and $PC_{71}BM$ is 2:8 (wt:wt %) fixed at a donor-to-acceptor ratio of 1:1.5 wt:wt% [19]. Alkylated-BT-substituted BDT-based **PBTBT-OTT**, which is extended in the 2D π-conjugation direction, exhibits the highest α and J_{SC} of our OSCs, and a PCE of 8.61%. This high PCE is mainly due to the increased α of the polymer, the complementary optical absorption properties of **PBTBT-OTT** and ITIC, the well-cascaded energy levels of **PBTBT-OTT**, ITIC, and $PC_{71}BM$, and the improved film morphology. The aim of this study was to investigate strategies for extending the π-conjugation length of the **PBT-OTT** backbone so as to achieve high-efficiency ternary-blend OSCs.

2. Results and discussion

2.1. Design, synthesis, and characterization of the polymer

The π-conjugated parent polymer **PBT-OTT** was systematically extended. A 1D backbone extension was achieved by fusing thiophenes onto both sides of the BDT structure (**PDTBT-OTT**). A 2D side-group extension was achieved by substituting 2-ethylhexyl BT for the 2-ethylhexyl selenophyl side group on the BDT unit of PBT-OTT to prepare **PBTBT-OTT**, and 2-ethylhexyl TT for the 2-ethylhexyl selenophyl side group on the BDT unit to prepare **PTTBT-OTT** (Scheme 1 and Table S1). These π-conjugated copolymers were synthesized by performing palladium-catalyzed Stille coupling reactions between the BDT and TPD derivatives (Scheme S1). The resulting crude copolymers were purified by successive washing with methanol, acetone, and hexane in a Soxhlet extractor.

The solubilities of the synthesized polymers are different: **PBT-OTT** and **PDTBT-OTT** have moderate solubility in chlorobenzene (CB) whereas **PTTBT-OTT** and **PBTBT-OTT** have limited solubility in CB but can be dissolved in 1,2-dichlorobenzene (DCB) to fabricate blend films. **PTTBT-OTT** dissolves at a higher temperature in DCB than **PBTBT-OTT**; this difference could be due to the rigid fused heteroaromatic BT and TT rings and the symmetric structure of TT, so the polymer based on 2-ethylhexyl-TT-substituted BDT is likely to exhibit lower solubility than the polymer based on 2-ethylhexyl-BT-substituted BDT.

The number molecular weights $\overline{Mn}$ and polydispersity indexes (PDIs) of the polymers were measured with gel permeation chromatography by using DCB as the eluent at 220 °C (Table S2). **PBT-OTT** has $\overline{Mn}$ = 23 kDa and PDI = 2.9; **PBTBT-OTT** has $\overline{Mn}$ = 26 kDa with PDI = 2.0, **PTTBT-OTT** has $\overline{Mn}$ = 24 kDa and PDI = 2.7, and **PDTBT-OTT** has $\overline{Mn}$ = 52 kDa with PDI = 2.0. The 1D π-conjugation-extended polymer **PDTBT-OTT** has the highest $\overline{Mn}$ of the synthesized polymers. This high $\overline{Mn}$ might arise because of the steric hindrance between the donor and acceptor derivatives in the **PDTBT-OTT** polymeric backbone (Section 2.3), which would increase its solubility in the reaction solvents (toluene and DMF) [24]. Therefore, the DTBT-OTT derivatives dissolve more in the reaction solvents during polymerization than the other derivatives, so **PDTBT-OTT** has the highest degree of polymerization.

All four polymers are thermally stable with decomposition temperatures T_d > 400 °C under a N_2 atmosphere (Fig. S1, Table S2); this result indicates that their thermal stabilities are high due to their extended

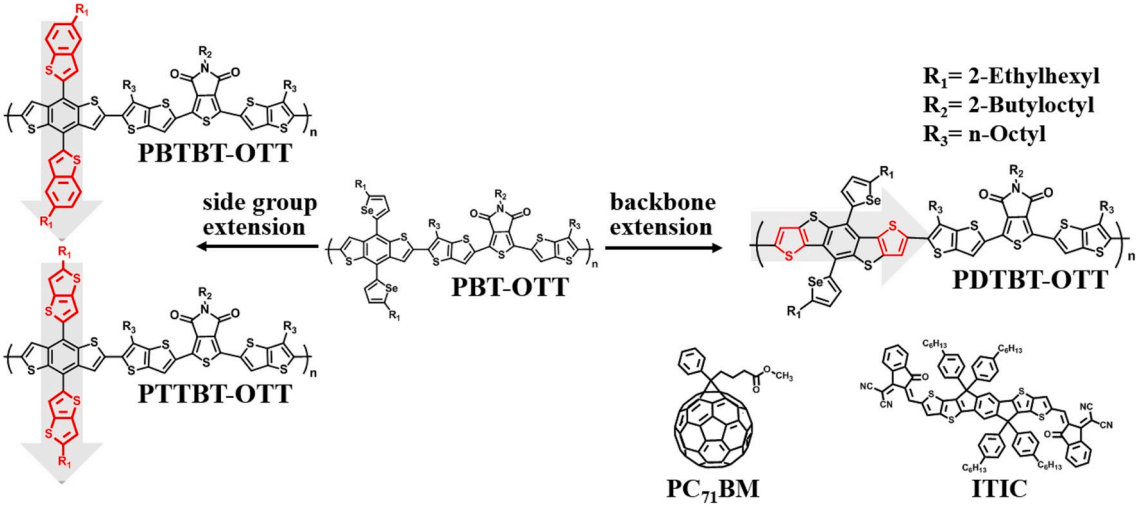

Scheme 1. Chemical structures of 1D or 2D π-conjugation-extended donor polymers, $PC_{71}BM$, and ITIC.

π-conjugation lengths. Therefore, the polymers have adequate thermal stabilities for use in optoelectronic devices [25]. No thermal transitions were found with differential scanning calorimetry for these polymers.

2.2. Optoelectrical properties

Cyclic voltammetry was conducted to estimate the HOMO energy levels of the polymers and ITIC, and their bandgaps E_g were used to determine their LUMO energy levels (Fig. 1a and Fig. S2). All HOMO levels were found to be increased by the 1D or 2D extensions of the **PBT-OTT** backbone π-conjugation length, except that of **PBTBT-OTT**. This increase is due to the electron-donating strength of the fused and substituted thieno[3,2-b]thiophene structure and their greatly extended

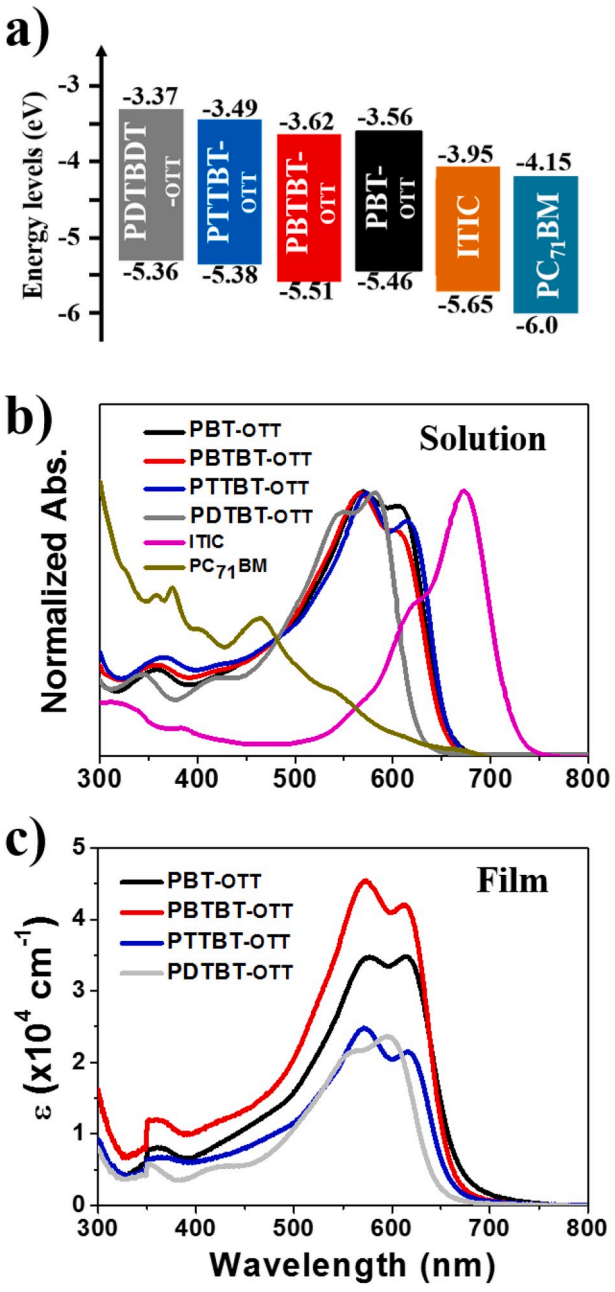

Fig. 1. a) Energy levels diagrams for synthesized polymers, ITIC, and $PC_{71}BM$, UV–Vis absorption and ITIC in b) solution and c) film; the ε in the legend represents absorption coefficient of the polymers. The thicknesses of the polymer films were 99 nm for PBT-OTT, 112 nm for PBTBT-OTT, 97 nm for PTTBT-OTT, and 106 nm for PDTBT-OTT.

π-conjugation systems [21,22,26]. Furthermore, extending the polymeric backbone (**PDTBT-OTT**) has a stronger effect on the HOMO energy level than extending the side group (**PTTBT-OTT**). On the other hand, the HOMO energy level of **PBTBT-OTT** is lower because of the addition of 2-ethylhexyl BT as a side group: the benzene ring is π−deficient when compared with a thiophene ring [27]. When conjugated polymer chains are fused to benzene, their electron density decreases; therefore, this decrease in the HOMO energy level will increase the open circuit voltage, V_{OC}, of the OSCs based on **PBTBT-OTT** (Section 2.5). By extending the π-conjugation length of **PBT-OTT**, the LUMO energy levels of the resulting polymers are upshifted in proportion to their E_g, but the opposite occurs in **PBTBT-OTT**. **PDTBT-OTT** has a higher LUMO energy level than the other polymers, possibly due to the significant increase in E_g resulting from the backbone conjugation extension. As a result, incorporating 2-ethylhexyl BT onto the BDT unit simultaneously decreases the HOMO and LUMO energy levels of **PBTBT-OTT**.

The cascade energy level alignment of the four polymers, ITIC, and the $PC_{71}BM$ neat film is shown in Fig. 1a. The HOMO and LUMO energy levels of ITIC lie between those of the four polymers and $PC_{71}BM$; this relationship means that holes are transferred efficiently from $PC_{71}BM$ and that electron transfer from the polymers is promoted.

The UV–Vis absorption spectra of solutions and thin films of these materials were determined in the visible region (Fig. 1b and c). The absorption spectra of the four polymers and ITIC contain strong absorptions with absorption maxima at ~ 600 nm (polymers) and 672 nm (ITIC) (Fig. 1b). Therefore, the absorption spectra of the polymers are complementary to that of ITIC, which extends into the near-infrared region; this complementarity means that the light harvesting of the ternary blends will be superior to that of their binary blends (polymer: $PC_{71}BM$) [19].

The absorption coefficient α of **PBTBT-OTT** is the highest of these polymers, followed by those of **PBT-OTT**, **PTTBT-OTT**, and then **PDTBT-OTT** (Fig. 1c). In the wavelength range (300–640 nm), the α of PBTBT-OTT was superior to that of other polymers. On the other hand, in the wavelength range (640 – 700 nm), the α of PBT-OTT was the highest. This trend in α is expected to be reflected in the J_{SC} values of the associated ternary OSCs (Section 2.5). When the 2D π-conjugation length is extended by using 2-ethylhexyl TT as a side group, the α value is decreased, possibly because the 2-ethylhexyl TT side groups reduce the crystallinity and thereby reduce the light absorption (Fig. 3a). Patterns of light absorption in conjugated polymers are affected by crystallinity of polymers as well as conjugation system of polymers [20,21,28,29] When 2-ethylhexyl BT is introduced, the resulting polymer **PBTBT-OTT** has a higher α than **PTTBT-OTT**. This increase might occur because not only π-conjugation length on **PBTBT-OTT** is extended from the parent polymer but also the crystallinity of **PBTBT-OTT** is superior to that of **PTTBT-OTT** (Fig. 3a).

After the introduction of the two thiophene groups, one on either side of the BDT unit copolymerized with TPD derivatives, the α value of the resulting 1D conjugation-extended **PDTBT-OTT** is lower than that of the parent polymer. This change might occur because the curved structure of the **PDTBT-OTT** backbone absorbs sunlight inefficiently [23]; this curved structure is due to the steric hindrance between the 2-ethylhexyl selenophyl side groups on the DTBT unit and the adjacent octyl chain on the TT π-bridge in the **PDTBT-OTT** backbone (Fig. S3). This steric hindrance increases E_g and blue-shifts the UV–Vis spectrum, and thus means that **PDTBT-OTT** has the lowest α value.

2.3. Theoretical calculations

To better understand the effects of π-conjugation extension on the molecular orbital distribution and molecular architecture of the polymers, density functional theory (DFT) calculations were performed with the B3LYP/6-31G* model [30–32]. To avoid excessive computation demand, the linear and branched alkyl chains on the polymeric

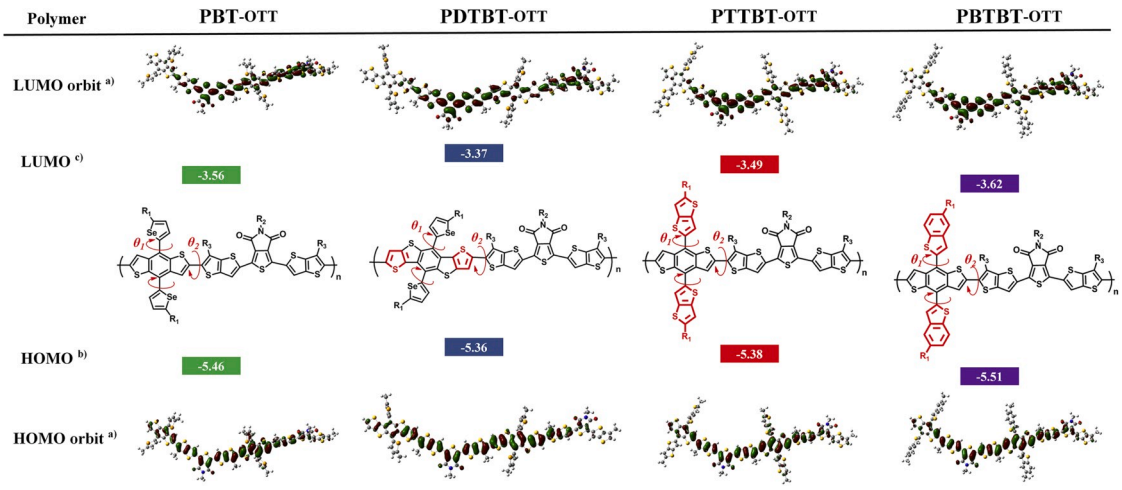

Fig. 2. (a) Energy-minimized structure (B3LYP/6-31G*) of the HOMO and LUMO of the trimer model compounds. (b) The HOMO energy levels were measured by cyclic voltammograms in thin film. (c) The LUMO energy is estimated by adding the absorption onset to the HOMO.

backbone were replaced with methyl groups, and the backbones were simplified to two repeating units (di-DTBT-OTT, di-BTBT-OTT, di-TTBT-OTT or di-BT-OTT) in optimized geometries in an energy-minimized structure (Fig. 2). For dimers, the HOMO wave functions are well delocalized along the dimeric backbones whereas their LUMO wave functions are more localized at the acceptor components (Fig. 2).

After extending the π-conjugation length, the dihedral angles θ_1 and θ_2 of the dimeric backbones were found to increase, where θ_1 is the dihedral angle between the side group and the BDT or DTBT unit and θ_2 is the dihedral angle between the BDT unit and the adjacent 3-octyl TT π-bridge (Fig. 2 and Table S3). When compared with di-BT-OTT, the 2D side group extensions with methyl TT and methyl BT slightly increase θ_1; they are 58.4° in di-BTBT-OTT, 57.0° in di-TTBT-OTT, and 54.8° in di-BT-OTT (Table S3); The θ_1 of di-BTBT-OTT is larger than that of di-TTBT-OTT because the methyl BT side-group is a larger than the methyl TT side group.

The 1D backbone extension through the introduction of the DTBT unit significantly increases θ_1 between methyl selenophene and the DTBT unit to 79.3° (Fig. 2, Table S3). This increase might occur because the shape of the dimeric backbone is changed from linear to curved, which induces much steric hindrance between the methyl selenophyl side group on DTBT and the adjacent methyl chain on the TT π-bridge (Fig. S3 and Table S3). This steric hindrance is likely to increase the twist in the polymeric backbone and to increase the θ_2 of the polymeric backbone of di-DTBT-OTT (Fig. 2 and Table S3). Furthermore, this effect may explain why for PDTBT-OTT E_g is wider and the UV–Vis absorption spectrum is blue-shifted.

Overall, the π-conjugation extensions through molecular engineering increase the dihedral angles θ_1 and θ_2 of the polymers by inducing steric hindrances. However, the influence of these steric hindrances is not so severe that it reduces the molecular orderings or charge carrier mobilities of the polymers.

2.4. Characteristics of OFETs based on these polymers

Organic field effect transistors (OFETs) were fabricated to evaluate how the 1D and 2D π-conjugation extensions of **PBT-OTT** affect the carrier transport properties of the polymers (Fig. 3 and Table S4). The

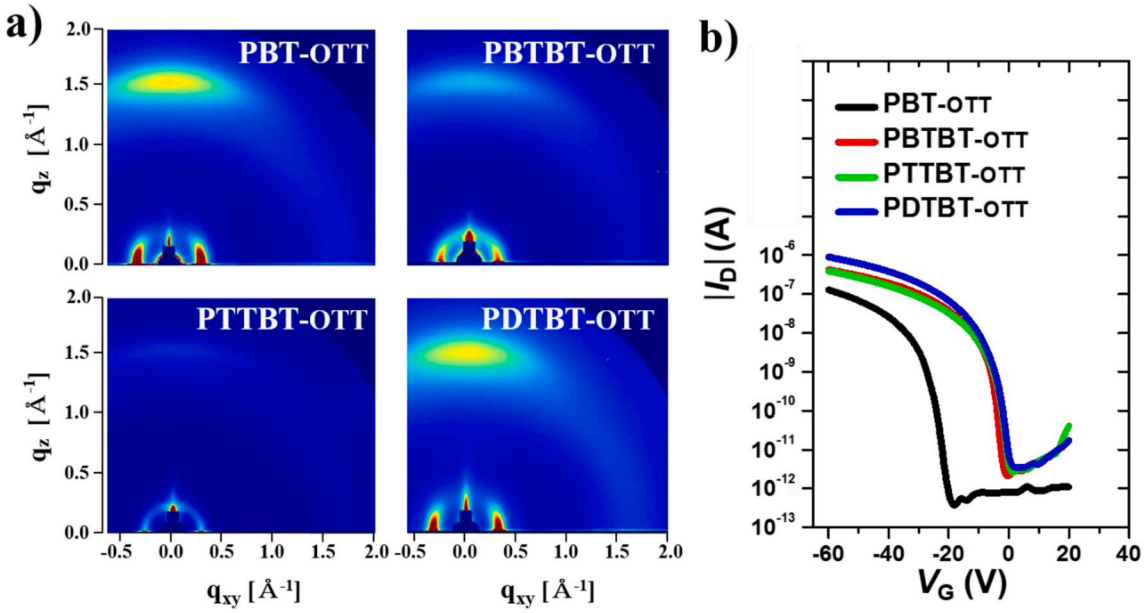

Fig. 3. a) GIWAXS patterns of polymer films and b) typical transfer curves of polymer based field effect transistors (thermal annealing of PBT-OTT at 240 °C, PBTBT-OTT at 180 °C, PTTBT-OTT at 280 °C, and PDTBT-OTT at 240 °C).

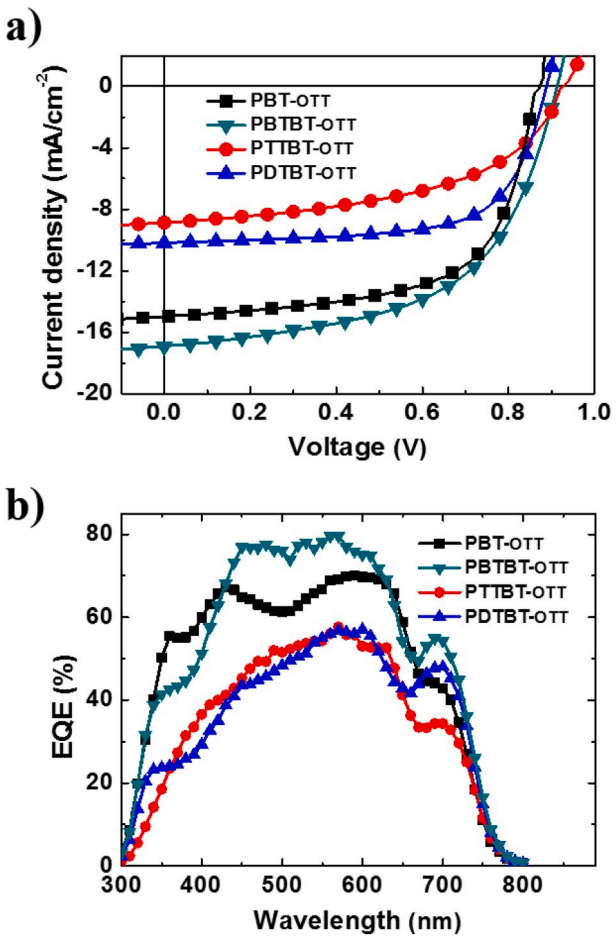

Fig. 4. Photovoltaic performance of the devices. a) Characteristic *J-V* curves of the devices based on polymers:$PC_{71}BM$ with 20 wt % of ITIC under illumination of AM 1.5 G, 100 mW/cm^2 light. b) EQE curves of the devices.

OFET hole mobilities μ_h of the polymers were optimized by carrying out thermal annealing. The calculated μ_h values of **PBT-OTT**, **PTTBT-OTT**, **PBTBT-OTT**, and **PDTBT-OTT** are 1.02×10^{-2}, 2.28×10^{-3}, 2.65×10^{-3}, and 9.45×10^{-3} cm^2 V^{-1} s^{-1}, respectively (Fig. S4 and Table S4). Thus, **PBT-OTT** exhibits the highest OFET μ_h of the polymers. Extending the π-conjugation lengths of **PBT-OTT** reduces μ_h because the 1D and 2D π-conjugation extensions increase the steric hindrance along the polymeric backbone and between the polymer chains.

To better understand the variation in the μ_h values of the OFETs that use the synthesized polymers, the crystalline ordering of each OFET active layer was examined with GIWAXS analysis (Fig. 3). The samples for the GIWAXS measurements were spin-coated from DCB solution onto SiO_2/Si substrates that had been treated with octadecyltrichlorosilane. The GIWAXS images (Fig. 3) show that all the polymers exhibit preferential face-on orientation; the intensity of the face-on orientation decreases in the order **PBT-OTT**, **PDTBT-OTT**, **PBTBT-OTT**, **PTTBT-OTT**.

The coherence lengths (CLs) of the polymers were calculated by using the Scherrer equation [33]. As the π-conjugation length increases, CL decreases: 94.5 Å for **PBT-OTT**, 94.4 Å for **PDTBT-OTT**, 88.8 Å for **PBTBT-OTT**, and 83.8 Å for **PTTBT-OTT** (Table S5). Increasing the CL of a polymer provides efficient π-π stacking channels that improve charge-carrier transport [34,35]. These results are consistent with the trend in μ_h for the OFETs based on the polymers. For example, the **PDTBT-OTT** polymer exhibits better charge carrier transport through the channels than the other polymers. Furthermore, the peak in the face-on orientation of **PDTBT-OTT** is higher in intensity than those of **PBTBT-OTT** and **PTTBT-OTT** after thermal annealing; this is the reason that μ_h for **PDTBT-OTT** is higher than those for **PBTBT-OTT** and **PTTBT-OTT**.

2.5. Photovoltaic properties of the OSCs

The effects of the π-conjugation extensions on the photovoltaic properties were investigated (Fig. 4 and Table 1). Upon the incorporation of $PC_{71}BM$ into the binary blends (polymer:ITIC), the resulting PCEs of the OSCs are enhanced due to increases in J_{SC} or FF (Table S6). It was found that the optimal overall donor-to-acceptor ratio in the active layer is 1:1.5 (wt:wt %) and that the optimal overall acceptor ratio of ITIC and $PC_{71}BM$ is 2:8 (wt:wt %). The OSCs based on **PBT-OTT** exhibit J_{SC} = 14.98 mA cm^{-2}, V_{OC} = 0.87 V, and FF = 62.6%, with PCE = 8.15%. The OSCs based on **PDTBT-OTT,** obtained by extending the 1D π-conjugation length with the DTBT derivative, exhibit reduced J_{SC} and PCE values. Extending the 2D π-conjugation by using 2-ethylhexyl TT or 2-ethylhexyl BT significantly reduces J_{SC} to 9.38 mA cm^{-2} and PCE to 4.23% in the OSCs based on **PTTBT-OTT**, and increases J_{SC} to 16.61 mA cm^{-2} and PCE to 8.61% in the OSCs based on **PBTBT-OTT**. The best characteristics are those of the OSCs based on **PBTBT-OTT**: J_{SC} = 16.61 mA cm^{-2}, V_{OC} = 0.92 V, and *FF* = 56.4% with PCE = 8.61%.

The OSCs based on **PBTBT-OTT** have the highest J_{SC} = 16.61 mA cm^{-2}, followed by the OSCs based on **PBT-OTT** (J_{SC} = 14.98 mA cm^{-2}), the OSCs based on **PDTBT-OTT** (J_{SC} = 9.79 mA cm^{-2}), and the OSCs based on **PTTBT-OTT** (J_{SC} = 9.38 mA cm^{-2}). This trend in J_{SC} mostly follows that in the light absorption of the corresponding polymers (Table 1 and Fig. 1c). The overall EQE is higher in the OSCs based on **PBTBT-OTT** than in the OSCs based on **PBT-OTT**. The high J_{SC} of the OSCs based on **PBTBT-OTT** is expected, because of its increased α (Fig. 1c). J_{SC} is slightly higher in the OSCs based on **PDTBT-OTT** than in the OSCs based on **PTTBT-OTT**, despite α being lower in **PDTBT-OTT** than in **PTTBT-OTT**; this trend arises because the OSCs based on **PDTBT-OTT** have a higher EQE than the OSCs based on **PTTBT-OTT** for the range $660 \leq \lambda \leq 800$ nm, which corresponds to the main absorption band of ITIC. As a result, the overall EQE of **PDTBT-OTT** is superior to that of **PTTBT-OTT** (Fig. 4b).

The V_{OC} values of the OSCs prepared from the π-conjugation-extended polymers are 0.87 V (**PBT-OTT**), 0.92 V (**PBTBT-OTT**), 0.90 V (**PTTBT-OTT**), and 0.86 V (**PDTBT-OTT**) (Table 2). V_{OC} is closely related

Table 1
Optical and electrochemical properties and related energy levels of the polymers and ITIC.

Polymer	λ_{max}, Soln. [nm]	λ_{max}, Film [nm]	λ_{onset}, Soln. [nm]	E_g[a] [eV]	HOMO[b] [eV]	LUMO[c] [eV]
PBT-OTT	569, 608	570, 611	652	1.90	−5.46	−3.56
PBTBT-OTT	567, 605	574, 613	655	1.89	−5.51	−3.62
PTTBT-OTT	571, 614	570, 617	655	1.89	−5.38	−3.49
PDTBT-OTT	546, 582	558, 594	623	1.99	−5.36	−3.37
ITIC	619, 672	–	730	1.70	−5.65	−3.95

[a] $E_g^{opt} = 1240/\lambda_{onset}$.
[b] HOMO = – (4.80 + E_{onset}, ox).
[c] LUMO = HOMO + E_g.

Table 2
Detailed photovoltaic parameters of ternary blend devices (polymer: ITIC:$PC_{71}BM$).

Polymer	DIO (%)	Thickness [nm]	J_{sc} [mA cm^{-2}]	V_{OC} [V]	FF [%]	PCE [%]
PBT-OTT	3	219	14.98	0.87	62.6	8.15
PBTBT-OTT	1	192	16.61	0.92	56.4	8.61
PTTBT-OTT	–	163	9.38	0.90	50.1	4.23
PDTBT-OTT	–	221	9.79	0.86	71.1	6.00

- ITIC:$PC_{71}BM$ (20:80 wt%).

to the energy difference between the HOMO energy level of the electron donor and the LUMO energy level of the electron acceptor. Extending the 2D π-conjugation length by using 2-ethylhexyl BT side groups results in a decrease in the HOMO energy level, so **PBTBT-OTT** has an increased V_{OC}. In contrast, extending the 1D π-conjugation length to produce **PDTBT-OTT** means that it has a higher HOMO energy level and a reduced V_{OC}. However, the HOMO energy levels and V_{OC} of **PTTBT-OTT** do not follow this pattern: extending the 2D π-conjugation length by using the 2-ethylhexyl TT side group leads to an increase in the HOMO energy level but also to an increase in V_{OC}. V_{OC} is high despite the increased HOMO energy level possibly because of the immiscible morphology of the **PTTBT-OTT** blend; immiscible ITIC domains could be present in the **PTTBT-OTT** blend that increase the overall LUMO energy level (Fig. 6).

The FF value of the OSCs based on **PDTBT-OTT** (71.1%) is the highest of the tested OSCs. The FF values of the OSCs based on the other polymers are as follows: **PBT-OTT**, 62.6%; **PBTBT-OTT**, 56.4%; **PTTBT-OTT**, 50.1%. The FF is determined by disproportionate charge collection with balanced charge transport. The balance between μ_h and the electron mobility μ_e in each active layer was investigated by using the space-charge limited current (SCLC) method for hole-only and electron-only devices (Fig. S4 and Table S7). The OSCs based on **PBT-OTT** exhibit FF > 60% because for these OSCs $\mu_h/\mu_e \approx 1$, which means that generated free charges can be extracted efficiently to the electrodes. The OSCs based on **PDTBT-OTT** exhibit FF > 70% because for these OSCs μ_e is higher, so $\mu_h/\mu_e \approx 1$. Although the OSCs based on **PBTBT-OTT** exhibit a relatively low FF, 56.4%, the OSCs based on this polymer exhibit a high μ_h and a reasonable $\mu_h/\mu_e = 0.83$. However, the OSCs based on **PTTBT-OTT** exhibit the lowest FF, 50.1%, and a μ_h/μ_e ratio that differs significantly from 1, possibly because there is poor phase separation in the **PTTBT-OTT** blend film. Accordingly, exciton dissociation does not occur efficiently in the active layers of OSCs based on **PTTBT-OTT** and so generated free charges accumulate.

2.6. Charge recombination dynamics

To characterize the charge-recombination dynamics of the OSCs, we measured the J_{SC} of each device as a function of the illumination intensity P_{light} (Fig. 5a). In principle, J_{SC} values in OSCs exhibit a power-law dependence on the light intensity P_{light}, i.e. $J_{SC} \propto (P_{light})^S$ [36,37]. Weak bimolecular recombination in the devices should produce a linear dependence of J_{SC} on P_{light}; i.e., $S \approx 1$. S is 0.990 in the OSCs based on **PBT-OTT** [19], 0.969 in the OSCs based on **PBTBT-OTT**, 0.912 in the OSCs based on **PTTBT-OTT**, and 0.993 in the OSCs based on **PDTBT-OTT** (Table S8); i.e., $S \approx 1$ for all the devices, except for the OSCs based on **PTTBT-OTT**. This result indicates that bimolecular charge recombination is negligible in the OSCs based on **PBT-OTT**, **PBTBT-OTT**, and **PDTBT-OTT**, but as a result of the 2D π-conjugation extension using 2-ethylhexyl TT, bimolecular recombination is enhanced in the OSCs based on **PTTBT-OTT**. These results for bimolecular recombination are well correlated with the μ_h values and μ_h/μ_e ratios obtained with SCLC, and with the FF values of the devices (Table S7).

The slope of the plot of V_{OC} versus log(P_{light}) helps to quantify the degree of trap-assisted recombination in the devices (Fig. 5b). A slope of k_BT/q implies whether trap-assisted recombination is the dominating mechanism or not, where k_B is Boltzmann's constant, T is absolute temperature and q is elementary charge. For trap-assisted or Shockley-Read-Hall recombination, V_{OC} is strongly dependent on the light intensity, and the slope is 2 k_BT/q [36–38]. For our polymers, the slope is 1.44 k_BT/q for the OSCs based on **PBT-OTT** [19], 1.74 k_BT/q for the OSCs based on **PBTBT-OTT**, 1.42 k_BT/q for the OSCs based on **PDTBT-OTT**, and 1.91 k_BT/q for the OSCs based on **PTTBT-OTT** (Table S8). These results indicate that the 1D π-conjugation extension reduces the trap densities between the active layer materials, i.e., in the OSCs based on **PDTBT-OTT**. In contrast, the films based on polymers with 2D π-conjugation extension using 2-ethylhexyl TT have morphologies with poor phase separation, so the trap density is increased. As a result of 2D π-conjugation extension with 2-ethylhexyl BT, the OSCs based on **PBTBT-OTT** do exhibit increased trap densities. However, the OSCs based on **PBTBT-OTT** still exhibit high J_{SC}, possibly because the high charge density that results from the high α of **PBTBT-OTT**

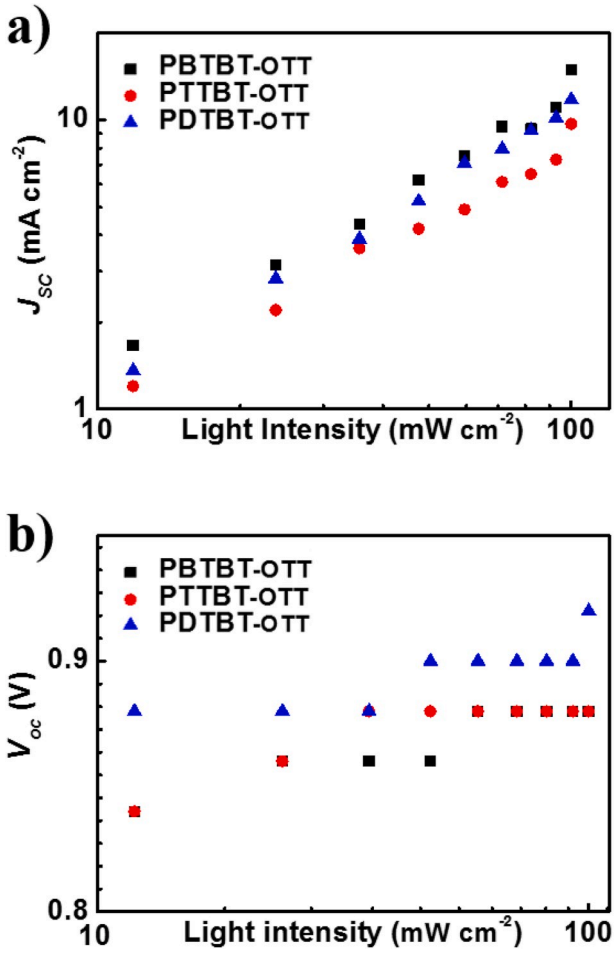

Fig. 5. a) Short-circuit current density (J_{SC}) versus light intensity and b) open-circuit voltage (V_{OC}) versus light intensity for the ternary blend OSCs.

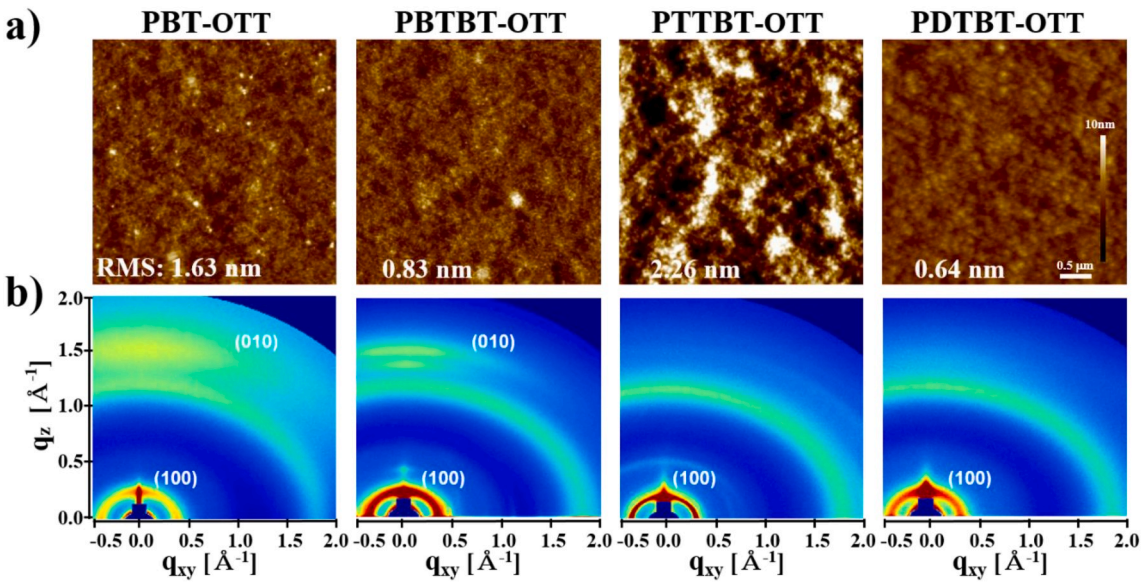

Fig. 6. a)AFM images and b) GIWAXS data of polymers:$PC_{71}BM$ blend films with 20 wt % ITIC.

compensates for the high interfacial surface trap density.

2.7. Thin film morphology and molecular ordering

Atomic force microscopy (AFM) analyses were performed to investigate how the π-conjugation extensions of the **PBT-OTT** backbone affect the blend film morphologies, and to characterize the relationship between these morphologies and the photovoltaic properties of the associated OSCs (Fig. 6a). As a result of the 1D extension of the π-conjugation length with the DTBT derivative, the surface of the **PDTBT-OTT** blend film is smooth and its root-mean-square surface roughness, RMS, is significantly lower, 0.64 nm compared to 1.63 nm (**PBT-OTT**) (Fig. 6a). As a result of the 2D extension of π-conjugation with the 2-ethylhexyl BT side group, the blend film forms a surface that is smoother (RMS = 0.83 nm for the **PBTBT-OTT** blend film) than that of the **PBT-OTT** blend film. However, the surface of the **PTTBT-OTT** blend film contains dramatically aggregated morphologies (RMS = 2.26 nm).

The aggregated morphology of the **PTTBT-OTT** blend film means that exciton dissociation does not occur efficiently and that electron transport pathways do not form [39]. Thus the 2D extension of the π-conjugation length through the introduction of an 2-ethylhexyl TT side group leads to an inferior surface morphology and poor electrical device characteristics. In contrast, the well-mixed morphologies of the **PDTBT-OTT** blend films favor efficient charge transport (Section 2.6), as demonstrated by the observation that its value of FF is the highest of the blend films. As a result, the PCE of the OSCs of the devices based on **PDTBT-OTT** is higher than that of the OSCs based on **PTTBT-OTT** (Table 2). The RMS of the **PBTBT-OTT** blend film with the best PCE and FF is slightly higher than that of the **PDTBT-OTT** blend film, so the morphology of the **PBTBT-OTT** blend film is favorable to better device efficiency.

To characterize the compatibility of each polymer with ITIC and $PC_{71}BM$, the surface energies γ^{total} of each polymer, ITIC, and $PC_{71}BM$ were measured (Table S9). The similarity of the surface energies of the polymer, $PC_{71}BM$, and ITIC results in good compatibility. The γ^{total} value that is closest to that of $PC_{71}BM$ and ITIC is $\gamma^{total} = 20.2$ mN m^{-1} for 1D π-conjugation-extended **PDTBT-OTT**, followed by **PBTBT-OTT** ($\gamma^{total} = 18.3$ mN m^{-1}), **PBT-OTT** ($\gamma^{total} = 17.6$ mN m^{-1}), and **PTTBT-OTT** ($\gamma^{total} = 16.9$ mN m^{-1}). Note that **PDTBT-OTT** is the most miscible with $PC_{71}BM$ and ITIC, and forms a well-mixed morphology. However, the morphologies of **PTTBT-OTT** were reversed in miscibility of **PTTBT-OTT** with $PC_{71}BM$ and ITIC.

GI-WAXS analyses were performed to characterize the polymer nanostructures and crystalline domains in the blend films (Fig. 6b). The films for the GIWAXS measurements were prepared from DCB blends on Si wafers coated with PEDOT:PSS. The crystal orientations of **PTTBT-OTT** and **PDTBT-OTT** are disturbed by the incorporation of ITIC and $PC_{71}BM$ (Fig. 3a vs Fig. 6b). As a result, the (100) crystal orientations of **PTTBT-OTT** and **PDTBT-OTT** in the blend films are randomized. No π-π stacking (010) peaks are evident, which degrades their charge transport and photovoltaic properties; this phenomenon may explain the poor PCEs of the devices that use this polymer film (Table 2). In contrast, the **PBT-OTT** and **PBTBT-OTT** blend films exhibit preferential face-on orientation with π-π stacking (010) peaks, which increase the favorability of intra-and intermolecular charge carrier transport in OSC devices [40–42]. Hence, the OSCs based on **PBT-OTT** and **PBTBT-OTT** exhibit high photovoltaic efficiencies. Note that peak π- π stacking of ITIC is evident in the **PBTBT-OTT** blend film, which can enhance light absorption by the main absorption band of ITIC, $660 \leq \lambda \leq 800$ nm (Fig. 4b). The sizes of the crystal domains of each polymer and of ITIC in the blend films were compared by using the Scherrer equation to calculate their coherence lengths (CLs) (Table S10). After blending with ITIC and $PC_{71}BM$, the CLs of the synthesized polymers decrease except for that of **PTTBT-OTT** (Table S4 and S10). The CL is largest in **PTTBT-OTT**, followed by **PBTBT-OTT**, **PBT-OTT,** and then **PDTBT-OTT**. These results are similar to those obtained for the blend film morphologies from the AFM images (Fig. 6a). It was implied that much larger CL of **PTTBT-OTT** in blends and dramatically aggregated morphologies (Table S10 and Fig. 6a) showed that exciton dissociation does not occur efficiently in the active layer of OSCs based on **PTTBT-OTT** due to the decreased area of the interface between the polymer and the acceptors (ITIC and $PC_{71}BM$) and the reduction in the number of free charge carriers due to geminate recombination. The large CL of ITIC can help to increase the light absorption of the **PBTBT-OTT** blend film, which might explain the increase in the intensity of the shoulder peak in its EQE in the range $660 \leq \lambda \leq 800$ nm (Fig. 4b). Thus, the OSCs based on **PBTBT-OTT** exhibit the highest photovoltaic efficiency of our synthesized-polymer-based OSCs because it has the highest α value and a large CL for ITIC, which promotes light absorption.

3. Conclusion

We systematically extended the π-conjugation length of a parent backbone in 1D and 2D directions. A series of wide bandgap D–A

copolymers, **PBT-OTT** (parent polymer), **PDTBT-OTT** (1D backbone extension consisting of the DTBT derivative), and **PTTBT-OTT** and **PBTBT-OTT** (2D side group extensions consisting of 2-alkyl TT and 2-alkyl BT respectively), based on the BDT donor moiety and the TPD acceptor moiety were synthesized by performing Stille coupling polymerizations under fixed conditions. Each polymer was blended with $PC_{71}BM$, then the narrow bandgap ITIC was incorporated into the blend. ITIC extends the light-absorption spectra of the blends and increases the photocurrent generation of the associated ternary-blend OSCs. The introduction of ITIC establishes an energy level cascade with each polymer and $PC_{71}BM$ to ensure efficient hole and electron charge transfer. The highest PCEs obtained with these OSCs are 8.15% (**PBT-OTT**), 6.00% (**PDTBT-OTT**), 4.23% (**PTTBT-OTT**), and 8.61% (**PBTBT-OTT**). In addition, the charge carrier transport properties of the resulting polymers are altered by the 1D and 2D π-conjugation extensions due to their effects on the polymeric steric hindrances. The side group extension of **PBT-OTT** with 2-alkyl BT increases the delocalization length along the 2D direction of the **PBTBT-OTT** backbone and effectively increases the absorption coefficient α; as a result, J_{SC} and PCE of the OSCs based on **PBTBT-OTT** are the highest for all the polymers. Furthermore, the π-deficient 2-alkyl BT side group in **PBTBT-OTT** gives it a deep HOMO energy level and thereby increases the V_{OC} value of the OSCs based on **PBTBT-OTT**. This improved morphology has the appropriate phase separation and preferential face-on orientation, which enables efficient exciton dissociation and free charge carrier transport. These results suggest that the π-conjugation extension of the **PBT-OTT** backbone provides a useful molecular engineering method for the development of high-efficiency OSCs.

Declaration of competing interest

The authors declare that they have no known competing financial interests or personal relationships that could have appeared to influence the work reported in this paper.

Acknowledgements

This work was supported by a grant (Code No. 2011-0031628) from the Center for Advanced Soft Electronics under the Global Frontier Research Program of the Ministry of Science and ICT, Korea. The authors thank the Pohang Accelerator Laboratory for providing the synchrotron radiation sources at 3C and 9A beamlines used in this study.

Appendix A. Supplementary data

Supplementary data to this article can be found online at https://doi.org/10.1016/j.orgel.2020.105738.

Author contributions

H. Hwang, C. Park, and D. H. Sin contributed equally to this work, which was supervised by K. Cho. H. Hwang synthesized all polymers used in this study. C. Park and D.H. Sin fabricated and characterized related photovoltaic devices. All authors contributed writing and reviewing the manuscript.

References

[1] D. Wöhrle, D. Meissner, Organic solar cells, Adv. Mater. 3 (1991) 129.
[2] S. Günes, H. Neugebauer, N.S. Sariciftci, Conjugated polymer-based organic solar cells, Chem. Rev. 107 (2007) 1324.
[3] M. Graetzel, R.A.J. Janssen, D.B. Mitzi, E.H. Sargent, Materials interface engineering for solution-processed photovoltaics, Nature 488 (2012) 304.
[4] A.C. Arias, J.D. MacKenzie, I. McCulloch, J. Rivnay, A. Salleo, Materials and applications for large area Electronics: solution-based approaches, Chem. Rev. 110 (2010) 3.
[5] S.B. Darling, F. You, The case for organic photovoltaics, RSC Adv. 3 (2013) 17633.
[6] Y. Cui, H. Yao, L. Hong, T. Zhang, Y. Xu, K. Xian, B. Gao, J. Qin, J. Zhang, Z. Wei, J. Hou, Achieving over 15% efficiency in organic photovoltaic cells via copolymer design, Adv. Mater. 31 (2019) 1808356.
[7] J. Yuan, Y. Zhang, L. Zhou, G. Zhang, H.-L. Yip, T.-K. Lau, X. Lu, C. Zhu, H. Peng, P. A. Johnson, M. Leclerc, Y. Cao, J. Ulanski, Y. Li, Y. Zou, Single-junction organic solar cell with over 15% efficiency using fused-ring acceptor with electron-deficient core, Joule 3 (2019) 1140.
[8] P. Cheng, Y. Li, X. Zhan, Efficient ternary blend polymer solar cells with indene-C60 bisadduct as an electron-cascade acceptor, Energy Environ. Sci. 7 (2014) 2005.
[9] Q. An, F. Zhang, J. Zhang, W. Tang, Z. Deng, B. Hu, Versatile ternary organic solar cells: a critical review, Energy Environ. Sci. 9 (2016) 281.
[10] L. Lu, M.A. Kelly, W. You, L. Yu, Status and prospects for ternary organic photovoltaics, Nat. Photon. 9 (2015) 491.
[11] Y. Gu, C. Wang, F. Liu, J. Chen, O.E. Dyck, G. Duscher, T.P. Russell, Guided crystallization of P3HT in ternary blend solar cell based on P3HT:PCPDTBT:PCBM, Energy Environ. Sci. 7 (2014) 3782.
[12] L. Lu, T. Zheng, Q. Wu, A.M. Schneider, D. Zhao, L. Yu, Recent advances in bulk heterojunction polymer solar cells, Chem. Rev. 115 (2015) 12666.
[13] S.M. Lee, T. Kumari, B. Lee, Y. Cho, J. Lee, J. Oh, M. Jeong, S. Jung, C. Yang, Horizontal-, vertical-, and cross-conjugated small molecules: conjugated pathway-performance correlations along operation mechanisms in ternary non-fullerene organic solar cells, Small (2020), 1905309-105309.
[14] H. Lu, J. Zhang, J. Chen, Q. Liu, X. Gong, S. Feng, X. Xu, W. Ma, Z. Bo, Ternary-blend polymer solar cells combining fullerene and nonfullerene acceptors to synergistically boost the photovoltaic performance, Adv. Mater. 28 (2016) 9559.
[15] J. Lee, S.M. Lee, S. Chen, T. Kumari, S.-H. Kang, Y. Cho, C. Yang, Organic photovoltaics with multiple donor–acceptor pairs, Adv. Mater. 31 (2019) 1804762.
[16] Y. Ma, Z. Kang, Q. Zheng, Recent advances in wide bandgap semiconducting polymers for polymer solar cells, J. Mater. Chem. A 5 (2017) 1860.
[17] Y. Li, M. Kim, Z. Wu, C. Lee, Y.W. Lee, J.-W. Lee, Y.J. Lee, E. Wang, B.J. Kim, H. Y. Woo, Influence of backbone modification of difluoroquinoxaline-based copolymers on the interchain packing, blend morphology and photovoltaic properties of nonfullerene organic solar cells, J. Mater. Chem. C 7 (2019) 1681.
[18] T. Liu, X. Xue, L. Huo, X. Sun, Q. An, F. Zhang, T.P. Russell, F. Liu, Y. Sun, Highly efficient parallel-like ternary organic solar cells, Chem. Mater. 29 (2017) 2914.
[19] H. Hwang, D.H. Sin, C. Park, K. Cho, Ternary organic solar cells based on a wide-bandgap polymer with enhanced power conversion efficiencies, Sci. Rep. 9 (2019) 12081.
[20] J.-H. Kim, J.B. Park, F. Xu, D. Kim, J. Kwak, A.C. Grimsdale, D.-H. Hwang, Effect of π-conjugated bridges of TPD-based medium bandgap conjugated copolymers for efficient tandem organic photovoltaic cells, Energy Environ. Sci. 7 (2014) 4118.
[21] H. Hwang, D.H. Sin, C. Kulshreshtha, B. Moon, J. Son, J. Lee, H.G. Kim, J. Shin, T. Joo, K. Cho, Synergistic effects of an alkylthieno[3,2-b]thiophene π-bridging backbone extension on the photovoltaic performances of donor–acceptor copolymers, J. Mater. Chem. A 5 (2017) 10269.
[22] Y.-X. Xu, C.-C. Chueh, H.-L. Yip, F.-Z. Ding, Y.-X. Li, C.-Z. Li, X. Li, W.-C. Chen, A. K.-Y. Jen, Improved charge transport and absorption coefficient in indacenodithieno[3,2-b]thiophene-based ladder-type polymer leading to highly efficient polymer solar cells, Adv. Mater. 24 (2012) 6356.
[23] J. Lee, J.-H. Kim, B. Moon, H.G. Kim, M. Kim, J. Shin, H. Hwang, K. Cho, Two-dimensionally extended π-conjugation of donor–acceptor copolymers via oligothienyl side chains for efficient polymer solar cells, Macromolecules 48 (2015) 1723–1735.
[24] J. Subbiah, B. Purushothaman, M. Chen, T. Qin, M. Gao, D. Vak, F.H. Scholes, X. Chen, S.E. Watkins, G.J. Wilson, A.B. Holmes, W.W.H. Wong, D.J. Jones, Organic solar cells using a high-molecular-weight benzodithiophene–benzothiadiazole copolymer with an efficiency of 9.4%, Adv. Mater. 27 (2015) 702.
[25] M. Jørgensen, K. Norrman, S.A. Gevorgyan, T. Tromholt, B. Andreasen, F.C. Krebs, Stability of polymer solar cells, Adv. Mater. 24 (2012) 580.
[26] J.-H. Kim, C.E. Song, B. Kim, I.-N. Kang, W.S. Shin, D.-H. Hwang, Thieno[3,2-b] thiophene-Substituted benzo[1,2-b:4,5-b′]dithiophene as a promising building block for low bandgap semiconducting polymers for high-performance single and tandem organic photovoltaic cells, Chem. Mater. 26 (2014) 1234.
[27] J. Wang, M. Xiao, W. Chen, M. Qiu, Z. Du, W. Zhu, S. Wen, N. Wang, R. Yang, Extending π-conjugation system with benzene: an effective method to improve the properties of benzodithiophene-based polymer for highly efficient organic solar cells, Macromolecules 47 (2014) 7823–7830.
[28] Y. Liu, J. Zhao, Z. Li, C. Mu, W. Ma, H. Hu, K. Jiang, H. Lin, H. Ade, H. Yan, Aggregation and morphology control enables multiple cases of high-efficiency polymer solar cells, Nat. Commun. 5 (2014) 5293.
[29] A.W. Birley, C. A. Daniels, Polymers: Structure and Properties, vol. 22, Technomic Publishing AG, Switzerland, 1990, ISBN 0-87762-552-2, pp. 261–262. British Polymer Journal.
[30] H. Hwang, H. Ko, S. Park, S.R. Suranagi, D.H. Sin, K. Cho, Fluorine-functionalization of an isoindoline-1,3-dione-based conjugated polymer for organic solar cells, Org. Electron. 59 (2018) 247.
[31] S.-W. Cheng, C.-E. Tsai, W.-W. Liang, Y.-L. Chen, F.-Y. Cao, C.-S. Hsu, Y.-J. Cheng, Angular-shaped 4,9-dialkylnaphthodithiophene-based donor–acceptor copolymers for efficient polymer solar cells and high-mobility field-effect transistors, Macromolecules 48 (2015) 2030–2038.
[32] J. Kim, K.-J. Baeg, D. Khim, D.T. James, J.-S. Kim, B. Lim, J.-M. Yun, H.-G. Jeong, P.S.K. Amegadze, Y.-Y. Noh, D.-Y. Kim, Optimal ambipolar charge transport of thienylenevinylene-based polymer semiconductors by changes in conformation for high-performance organic thin film transistors and inverters, Chem. Mater. 25 (2013) 1572.

[33] R.C. Raju Nagiri, S.D. Yambem, Q. Lin, P.L. Burn, P. Meredith, Room-temperature tilted-target sputtering deposition of highly transparent and low sheet resistance Al doped ZnO electrodes, J. Mater. Chem. C 3 (2015) 5322–5331.
[34] S. Wang, S. Fabiano, S. Himmelberger, S. Puzinas, X. Crispin, A. Salleo, M. Berggren, Experimental evidence that short-range intermolecular aggregation is sufficient for efficient charge transport in conjugated polymers, Proc. Natl. Acad. Sci. 112 (2015) 10599.
[35] H. Bin, Y. Yang, Z.-G. Zhang, L. Ye, M. Ghasemi, S. Chen, Y. Zhang, C. Zhang, C. Sun, L. Xue, C. Yang, H. Ade, Y. Li, 9.73% efficiency nonfullerene all organic small molecule solar cells with absorption-complementary donor and acceptor, J. Am. Chem. Soc. 139 (2017) 5085.
[36] I. Riedel, J. Parisi, V. Dyakonov, L. Lutsen, D. Vanderzande, J.C. Hummelen, Effect of temperature and illumination on the electrical characteristics of polymer–fullerene bulk-heterojunction solar cells, Adv. Funct. Mater. 14 (2004) 38.
[37] S.R. Cowan, A. Roy, A.J. Heeger, Recombination in polymer-fullerene bulk heterojunction solar cells, Phys. Rev. B 82 (2010) 245207.
[38] L.J.A. Koster, V.D. Mihailetchi, R. Ramaker, P.W.M. Blom, Light intensity dependence of open-circuit voltage of polymer:fullerene solar cells, Appl. Phys. Lett. 86 (2005) 123509.
[39] P. Kumar, Organic Solar Cells, CRC Press, Boca Raton, 2016, https://doi.org/10.1201/9781315370774.
[40] J. Shin, M. Kim, B. Kang, J. Lee, H.G. Kim, K. Cho, Impact of side-chain fluorination on photovoltaic properties: fine tuning of the microstructure and energy levels of 2D-conjugated copolymers, J. Mater. Chem. A 5 (2017) 16702.
[41] H. Bin, Z.-G. Zhang, L. Gao, S. Chen, L. Zhong, L. Xue, C. Yang, Y. Li, Non-fullerene polymer solar cells based on alkylthio and fluorine substituted 2D-conjugated polymers reach 9.5% efficiency, J. Am. Chem. Soc. 138 (2016) 4657.
[42] M.-H. Jao, H.-C. Liao, W.-F. Su, Achieving a high fill factor for organic solar cells, J. Mater. Chem. A 4 (2016) 5784.